# Graphene-Based Star–Mesh Resistance Networks

Dean G. Jarrett, *Senior Member, IEEE*, Ching-Chen Yeh, Shamith U. Payagala, Alireza R. Panna, Yanfei Yang, *Member, IEEE*, Linli Meng, Swapnil M. Mhatre, Ngoc Thanh Mai Tran, Heather M. Hill, Dipanjan Saha, Randolph E. Elmquist, *Senior Member, IEEE*, David B. Newell, and Albert F. Rigosi, *Member, IEEE*



***Abstract*— Advances in the development of graphene-based technology have enabled improvements in dc resistance metrology. Devices made from epitaxially grown graphene (EG) have replaced the GaAs-based counterparts, leading to an easier and more accessible realization of the ohm. By optimizing the scale of the growth, it has become possible to fabricate quantized Hall array resistance standards (QHARS) with nominal values between 1 kΩ and 1.29 MΩ. One of these QHARS device designs accommodates a value of about 1.01 MΩ, which made it an ideal candidate to pursue a proof-of-concept that graphene-based QHARS devices are suitable for forming wye–delta ($Y$–Δ) resistance networks. In this work, the 1.01-MΩ array output is nearly 20.6 MΩ due to the $Y$–Δ transformation, which itself is a special case of star–mesh transformations. These mathematical equivalence principles allow one to extend the quantized Hall resistance (QHR) to the 100-MΩ and 10-GΩ resistance levels with fewer array elements than would be necessary for a single array with many more elements in series. The 1.01-MΩ device shows promise that the $Y$–Δ transformation can shorten the calibration chain, and, more importantly, provide a chain with a more direct line to the quantum SI.**

***Index Terms*— Electrical measurement standards, epitaxial graphene, quantized Hall resistance (QHR), quantum Hall array resistance standard, wye–delta ($Y$–Δ) transformation.**

## I. Introduction

QUANTIZED Hall array resistance standards (QHARS) are devices that have been designed to accommodate many smaller elements that each output a resistance that is a multiple, integer or fractional, of $h/e^2$, where $h$ is the Planck constant, and $e$ is the elementary charge, respectively. Historically, QHARS were made with GaAs/AlGaAs heterostructures until they were replaced by graphene for metrology applications in the United States [1], [2], [3]. The ease of use associated with using graphene-based devices quickly caught on [4], [5], [6], with many groups worldwide using epitaxially grown graphene (EG) as a quantized Hall resistance (QHR) standard. Most graphene-based standards operate at the resistance plateau formed by the $\nu = 2$ Landau level (about 12906.4037 Ω) since that plateau is easier to access than the $\nu = 6$ plateau or others exhibited by graphene [7].

Assembling series and parallel connections of many Hall bars is now a promising avenue of research due to improved device geometries and superconducting electrical contacts between elements [8], [9], [10]. By adding sufficient elements in series, one may be able to shorten the chain of calibration by having higher quantized resistances. For instance, an array device valued at around 1 MΩ would require a minimum of 78 elements. Though feasible, engineering issues for even higher resistances compound rapidly since those higher decades, namely that 10 MΩ and beyond, would require an order of magnitude increase in the number of elements. For instance, it would require approximately 7748 array elements in series (assuming $\nu = 2$ quantization) to make an array of nearly 100 MΩ. This rapidly growing number of required elements for higher resistances presents a formidable engineering challenge.

To circumvent this scaling problem, QHARS devices were constructed with designs suitable for use in a wye–delta ($Y$–Δ) network. QHARS have been used for several efforts in resistance metrology, both of the graphene and GaAs/AlGaAs variety [8], [9], [10], [11], [12], [13], [14]. The exemplary 1.01-MΩ device has two arrays of 39 elements each connected in series with a single element connected at the midpoint to provide a way to check the quantization of each 39-element array. These three arms of the 1.01-MΩ device, by using the $Y$–Δ transformation, form higher resistance standards when compared to the three, relatively smaller, components. Due to the electrical and mathematical equivalence of the $Y$–Δ networks, this transformation can be used to construct standards with values between megaohms and gigaohms [15], [16]. The idea of using QHARS to form a $Y$–Δ transfer standard may be expanded to include future QHARS devices with transformed values of 100 MΩ and 10 GΩ with only several hundreds of elements, far fewer than the much larger numbers of 7748–7.75 × $10^5$ devices in series, respectively.

For this work, several 1.01-MΩ devices were fabricated at the National Institute of Standards and Technology (NIST) for calibrating 10-MΩ, 100-MΩ, and 1-GΩ resistance standards directly with a two-terminal cryogenic current comparator (CCC) [17] in a single step, without having to do two steps

Manuscript received 18 February 2023; revised 23 May 2023; accepted 10 June 2023. This work was supported by the U.S. Government. The Associate Editor coordinating the review process was Dr. Isaac Fan. *(Corresponding author: Dean G. Jarrett.)*

Dean G. Jarrett, Shamith U. Payagala, Alireza R. Panna, Heather M. Hill, Dipanjan Saha, Randolph E. Elmquist, David B. Newell, and Albert F. Rigosi are with the National Institute of Standards and Technology, Gaithersburg, MD 20899 USA (e-mail: dean.jarrett@nist.gov).

Ching-Chen Yeh and Swapnil M. Mhatre are with National Taiwan University, Taipei City 10617, Taiwan (e-mail: ching-chen.yeh@nist.gov).

Yanfei Yang and Linli Meng are with Graphene Waves, LLC, Gaithersburg, MD 20899 USA (e-mail: yanfei.yang@graphenewaves.com).

Ngoc Thanh Mai Tran is with the Joint Quantum Institute, University of Maryland, College Park, MD 20742 USA (e-mail: ngocthanhmai.tran@nist.gov).

Digital Object Identifier 10.1109/TIM.2023.3290290

from a single Hall bar element. A dual-source bridge (DSB) is also employed to measure the equivalent $Y$–$\Delta$ resistance of about 20.6 MΩ, proving that this overall concept is beneficial to future resistance metrology applications.

## II. Device Fabrication and Characterization

### A. Epitaxial Graphene Growth and Device Fabrication

Graphene films were grown on 22.8 × 22.8 mm silicon carbide chips. The chip was diced from a semi-insulating SiC wafer of diameter 10.2 cm (about 4 in) from Wolfspeed (see Acknowledgment for commercial disclaimer and the Appendix for growth information). The sample was cleaned with Piranha solution (3:1 $H_2SO_4$:$H_2O_2$) for 33 min at 120 °C, followed by a 5-min clean with 51% hydrofluoric acid (by volume and diluted with deionized water). Moments before the growth process was initiated; the chip was coated with a dilute solution of carbon-based photoresist (AZ 5214E, see Acknowledgment) in isopropanol to take advantage of the benefits of polymer-assisted sublimation growth (PASG) [18]. The graphite-lined resistive-element furnace (Materials Research Furnaces Inc., see Acknowledgment) was flushed with Ar gas and filled to about 103 kPa from a 99.999% liquid argon source before being held at about 1850 °C for 4 min [19], [20]. The chip with grown EG was removed after the system was allowed to cool to room temperature.

The grown EG samples were characterized using both optical and confocal laser scanning microscopy (CLSM). High-resolution confocal images have been taken at more than ten sampling sites (marked by the orange, green, and
AQ:6 red squares in Fig. 5 in the Appendix) for a quick evaluation of the variation of graphene thickness across the chip. More coverage information is available in the Appendix. Eight 1.01-MΩ devices have been fabricated in the region with minimum multilayers.

The device fabrication is similar to others reported in recent articles, whereby the EG layer has a 20-nm layer of Pd/Au deposited on it, followed by photolithography processes for defining the Hall bar and device contacts [7], [21], [22]. Though the intrinsic electron density in epitaxial graphene on SiC is near $10^{13}$ cm$^{-2}$, it is greatly reduced after the Pd/Au layer is removed by aqua regia [7], due to a p-doping process by the nitric acid [22]. The 1.01-MΩ devices are exposed to ambient air after fabrication so that the adsorption of oxygen molecules from the air will further p-doped graphene below $10^{11}$ cm$^{-2}$. Gently annealing the devices in a vacuum at a temperature of about 85 °C will release oxygen molecules slowly and the desired carrier density can be obtained by controlling the annealing time [22].

For the electrical contacts of the QHARS devices, a layer of superconducting NbTiN was deposited to greatly improve array performance [9]. Moreover, the contacts' design of incorporating a multiseries connection was critical to device functionality (see the Appendix for optical and CLSM images of the device), namely, to eliminate uncertainty due to lead resistances and to optimize the current flow [9]. The separation of the NbTiN layer and the EG was greater than 80 nm so that undesired quantum effects, such as Andreev reflection, could be prevented.

### B. Checking Material Homogeneity

Testing material homogeneity is crucial for ensuring a fully quantized device. After the first inspection done during the fabrication process, which involved CLSM and optical microscopy, a second, noninvasive inspection for homogeneity was performed via Raman spectroscopy given the potentially high doping [23], [24]. The optical properties of the EG also give an insight into the quality of the material that could have been overlooked. The Raman measurements were performed with a Renishaw InVia micro-Raman spectrometer (see Acknowledgment). A helium-neon laser, with an excitation wavelength of 633 nm, was used as the source. Each spectrum was measured using a backscattering configuration, 2-$\mu$m spot size, 1-mW power, 50 × objective, 300-s acquisition time, and 1200-mm$^{-1}$ grating. More information is provided in the Appendix.

## III. Verification and Measurement Methodology

### A. Intended Device Functionality

The aforementioned 1.01-MΩ device is intended to act as an unknown resistor, or rather, a resistor whose value is to be determined through this experiment and compared with what its quantized value should be. Each of its two arrays, composed of 39 elements each and connected in series, meets at a common node with a single element. The two equivalent arms nearly 0.5 MΩ each, along with the single element, make up the three resistors of a Y-network (designated $R_X$, Hi–Lo–Gnd, or $R_1$–$R_2$–$R_0$) and can be equated to three resistors arranged as a triangular mesh containing one less node than the Y-network (designated $R$, $R_a$, and $R_b$, where the latter two are inconsequential to the desired measurement). This equivalence is shown in Fig. 1(a) and is the essence of the $Y$–$\Delta$ transformation [15], which itself is a special case of star–mesh transforms [25], [26], [27]. These star–mesh transforms are used to reduce the number of nodes by 1. More details on cases beyond the triangular ($\Delta$) cases will be provided later. Depending on the values of the Y resistors, one can achieve higher, equivalent, and quantized resistances with simple mathematical formulae

$$
\begin{aligned}
R &= \frac{R_1 \times R_2}{R_0} + R_1 + R_2 \\
R_a &= \frac{R_1 \times R_0}{R_2} + R_1 + R_0 \\
R_b &= \frac{R_2 \times R_0}{R_1} + R_2 + R_0.
\end{aligned} \tag{1}
$$

It follows from (1) that in order to maximize the transformation for $R$, it would benefit greatly if one were to minimize $R_0$ given that it is the denominator. The $R_0$ arm is thus, arguably, the most influential piece of the Y configuration.

When configured properly and calculated via $Y$–$\Delta$ transform as shown in Fig. 1(b), the QHARS device yields an equivalent resistance $R$ of about 20.6 MΩ. This higher value could be used for calibrating 100-MΩ and 1-GΩ high resistance standards with a DSB having a 5:1 or 50:1 ratio, respectively [15], [28]. The 1.01-MΩ device is also designed to eventually be used with a two-terminal CCC as

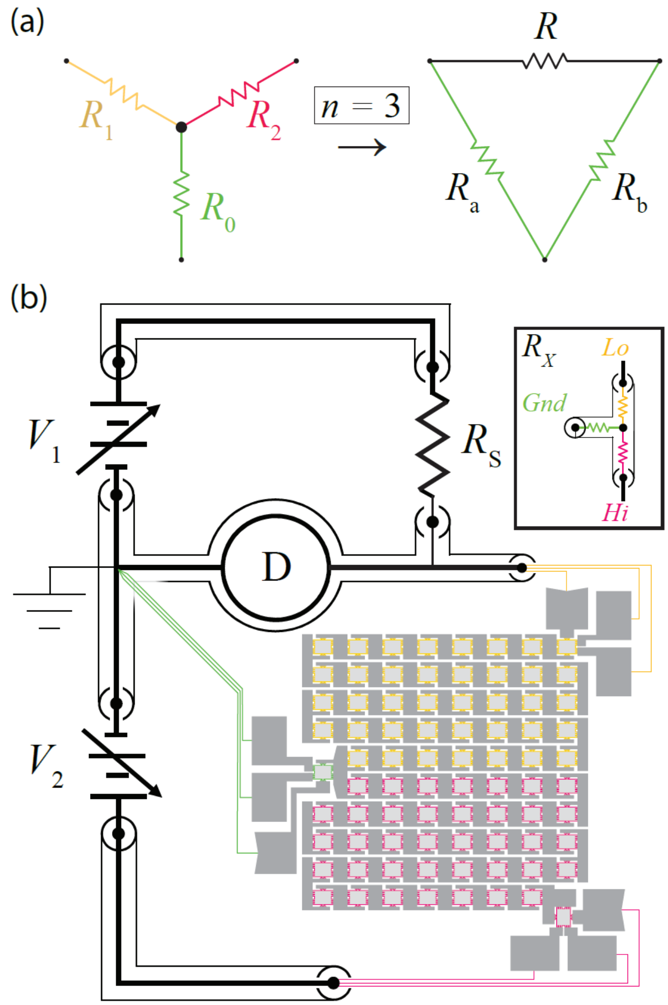


Fig. 1. (a) Illustration of the $Y$–$\Delta$ transformation is provided, reflecting the experimental setup. This transformation is a special case of the star–mesh transformation, which reduces the number of nodes by generating an equivalence resistance network. (b) Simplified diagram for experimental methods involving the use of a DSB. The top arm applies a voltage $V_1$ across a known reference resistance $R_S$, while the lower arm applies voltage $V_2$ with opposite polarity across an unknown resistor $R_X$. The voltage is then modified until the detector (labeled D) reads a null signal. The 1.01-MΩ device is intended to substitute $R_X$ (see upper inset), with each of its two arrays, composed of 39 elements each and connected in series, meeting at a common node with a single element. The single element represents the Gnd (or $R_0$, color-coded green), whereas the two larger arms make up the Lo and Hi ($R_1$ and $R_2$, respectively) terminal connections. It should be noted that a typical DSB setup has the unknown resistance $R_X$ on the top circuit and $R_S$ on the bottom circuit.

a means of scaling directly to higher resistances of 10 MΩ, 100 MΩ, and 1 GΩ with CCC turn-winding ratios of 10:1 or 100:1 [17], [29].

With relatively minor modifications in fabrication, similar array networks can be made for resistance values closer to decade values. Table I shows a few possible $Y$–$\Delta$ transformations that could generate a resistance $R$ for a QHARS device of corresponding design elements. These future QHARS devices may yield values closer to 100 MΩ and up to 10 GΩ using the $Y$–$\Delta$ transformation. In the case of a 10-GΩ equivalent resistance, an QHARS device would need to accommodate 501 elements, which is not an unreasonable projection given recent developments using several hundred [14]. The $R_1$ and $R_2$ arms in Table I mainly have elements in series, but it is possible to introduce one or more smaller parallel resistors (increasing the number of nodes—see the Appendix) to finely tune the desired equivalent resistance.

TABLE I
$Y$–$\Delta$ TRANSFORMATIONS FOR FUTURE QHARS DEVICES

| R1 (elements) | R2 (elements) | R0 (elements) | Total (elements) | R (MΩ) |
|---|---|---|---|---|
| 39 | 39 | 2 | 80 | 10.8220 |
| 39 | 39 | 1 | 79 | 20.6373 |
| 50 | 50 | 1 | 101 | 33.5566 |
| 60 | 60 | 1 | 121 | 48.0118 |
| 80 | 80 | 1 | 161 | 84.6660 |
| 96 | 79 | 1 | 176 | 100.141 |

### B. Dual Source Bridge and Transport Setup

To validate predictions obtained with the $Y$–$\Delta$ transformations, most measurements were performed using a DSB. Fig. 1(b) shows a DSB, also known as a modified Wheatstone bridge, which has been implemented in the past at various National Metrology Institutes [28], [29], [30], [31]. Generally, on the top arm, a voltage $V_1$ may be applied across a known reference resistance $R_S$, while on the lower arm, a voltage $V_2$ may be applied with opposite polarity across an unknown resistor $R_X$. In a DSB, $R_X$ or $R_S$ may be in either the upper or lower arm since $V_1$ and $V_2$ are interchangeable programmable voltage sources. Here, the reference resistor $R_S$ is used to evaluate the QHARS $R_X$. To calibrate a higher value standard resistor, the QHARS would be the standard $R_S$ and a high-value resistor would be the unknown $R_X$. The voltage is then adjusted until the detector (labeled D) reads a null signal.

A significant benefit of using a DSB is the very low uncertainties that can be achieved due to the simple calibration of the applied voltages. In addition, leakage effects become negligible since the sensitive bridge point detector gets balanced to a null current and the low impedance (<0.1 Ω at dc) of the voltage sources. The main uncertainties are the calibration of the voltage sources, offset voltages, noise, and reference resistor $R_S$.

Accurate measurements of Y-networks (also called T-networks) using a DSB require the Lo terminal $R_2$ to be at the same potential as that of the GND terminal on $R_0$. tetrahedral junctions [32] have been used to connect the three sets of triple-series leads from the QHARS to the DSB. By adding another tetrahedral junction at the bridge ground node, we plan to further suppress potential differences in the Lo leads of the detector, voltage sources, and $R_0$ leads from the QHARS.

Three resistors ($R_1$, $R_2$, and $R_0$) comprise the unknown resistance $R_X$, as shown in Fig. 1(b). The 1.01-MΩ device is put in the place of $R_X$ (see the upper inset), with each of its two arrays, composed of 39 elements each and connected in series, meeting at a common node with a single element. The single element (valued at about 12.9 kΩ) represents the Gnd terminal (or $R_0$, color-coded green), whereas the two larger arms make up the Hi and Lo ($R_1$ and $R_2$, respectively) terminal connections.

In terms of the upper arm, which hosts the reference resistor $R_S$, calibration was necessary in order to accurately measure the QHARS device's transformed quantized value. As such, $R_S$ was calibrated against the NIST QHR national standard with corresponding resistance bridges (and were valued at 1 and 10 MΩ). This calibration history spans years and includes calibration data taken with both graphene- and GaAs-based QHRs. Both resistors have drift rates of 0.7 ($\mu\Omega/\Omega$)/yr or less and temperature coefficients of 0.2 ($\mu\Omega/\Omega$)/°C or less. The drift rates were determined by linear regression of historical data and the resistors' temperature was controlled to within ±0.01 °C of 23 °C.

Before these high-resistance experiments can commence, one preferred step for all QHARS devices is to assess their transport properties. This preliminary step helps optimize the use of the more complicated DSB setup and measurements. These more basic quantum Hall transport measurements were performed with a Cryomagnetics C-Mag $^4$He cryostat (see the Acknowledgment). All devices were mounted onto a transistor outline (TO-8) package, and all corresponding magnetoresistance data were collected between magnetic field values of 0 and 8 T and at 2 K.

## IV. Measurement Results and Discussion

### A. Checking the QHARS Device Resistance

A pair of basic transport measurements is shown in Fig. 2(a). The two values were measured to be close enough to their nominal values (corresponding to 78 and 40 elements for the black and red curves, respectively) that precision measurements were then warranted. The magnetoresistances in Fig. 2(a) were collected with an HP 3458 digital voltmeter (see Acknowledgment). Though this technique allows one to collect data with higher magnetic field resolution, it potentially introduces small errors due to equipment impedance.

To perform a more precise measurement of the 1-MΩ QHARS, a CCC was used to make a two-terminal measurement. A nominal turns' ratio of 780:10, with a primary current of 0.775 $\mu$A, was applied to a 12.906-kΩ standard resistor using a cycle time of 60 s. A nominal current of 10 nA was applied to the 1-MΩ QHARS which was at a temperature of about 2.5 K, while the magnetic field was swept from ±2.8 to ± 9 T. The 30 CCC measurements were made at each magnetic field, with the last 16 measurements averaged for each field. Deviations from the nominal quantized value for the Hi–Lo 1-MΩ array are plotted in Fig. 2(b) and show a comfortable approach to quantization just under 4 T.

The difference between the plateaus obtained at opposite magnetic polarities is plotted in red with a right-side vertical axis. It is important to note the difference observed and its history of having been discussed in other work [33]. The device may not have been fully quantized, or a connection problem may have existed. When the field is reversed, the current goes through a different set of contacts, and the two-terminal CCC measurement is more susceptible to these possible differences in contact resistance.

After the precision measurements demonstrated the metrological viability of the QHARS subarrays, the device was implemented into the DSB setup, as shown in Fig. 1(b).

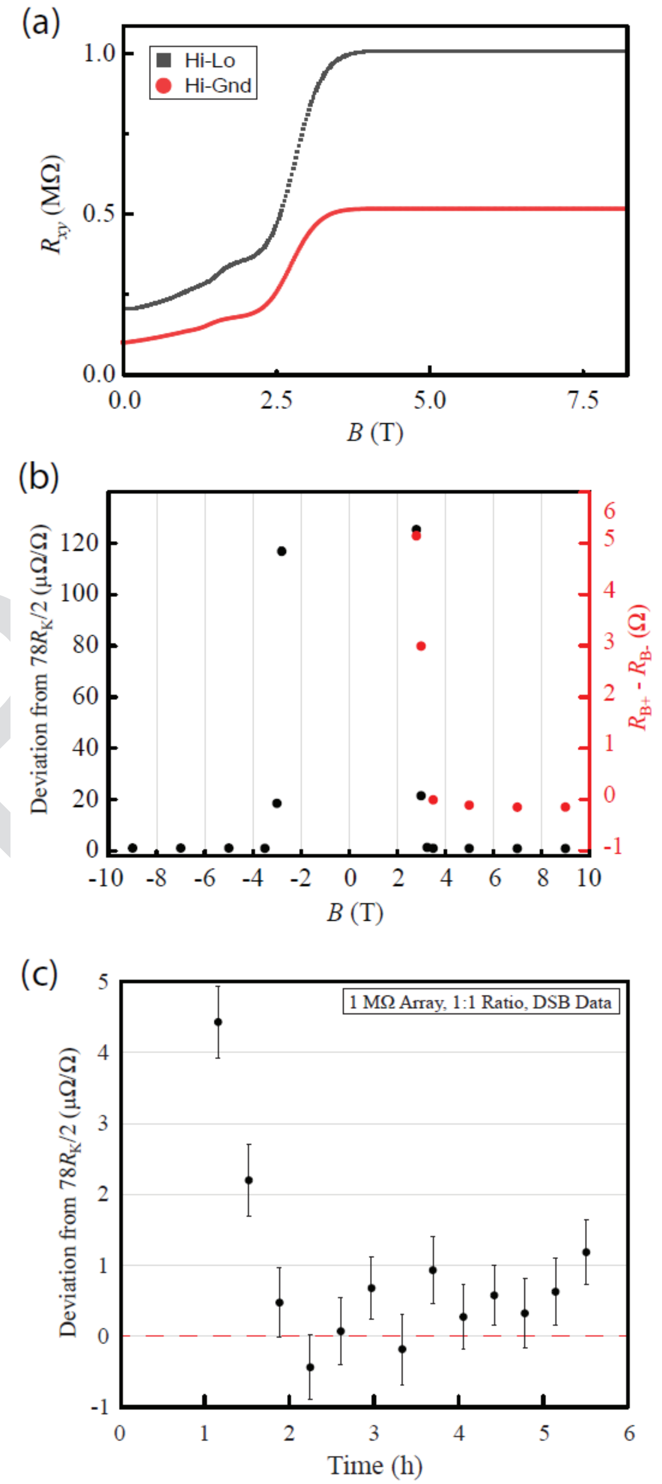


Fig. 2. (a) Basic transport measurements collected with an HP 3458 digital voltmeter. On the plateau (whose onset is about 4 T), the two values were measured to be close to their nominal values within the measurement capability, as seen by the Hi–Lo (78 elements, black curve) and Hi–Gnd (40 elements, red curve). (b) CCC measurements taken at various magnetic field values verified the quantization of the QHARS device. The difference between the plateaus of opposite magnetic polarities is plotted in red with a right-side vertical axis. Error bars for data are smaller than the points. (c) Time-dependent DSB measurements are shown and use a 1:1 ratio against the reference resistor. Error bars represent the combined standard uncertainty ($k = 1$).

The balancing results of this method, which reflect a 1:1 ratio against the reference resistor, are shown in Fig. 2(c). This

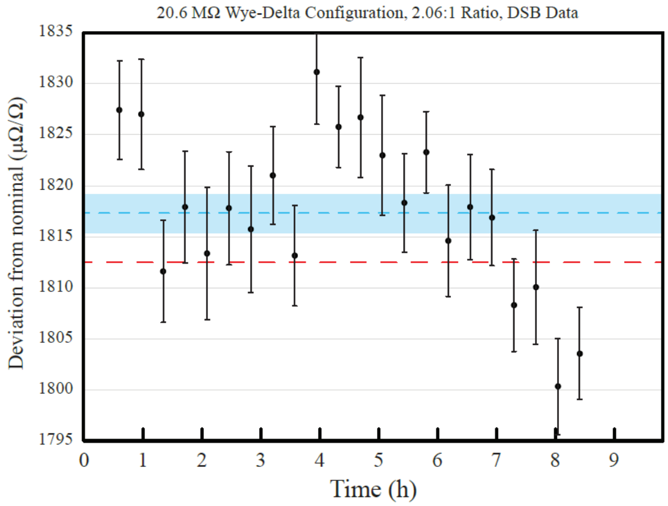


Fig. 3. Based on the $Y$–$\Delta$ transformation calculation, the 1.01-MΩ QHARS device was predicted to exhibit a resistance nearly 20.6 MΩ when in a proper configuration. A 10-MΩ resistor was used as $R_S$ in order to apply a voltage ratio of about 2.06:1. The time-dependent results have shown a necessary settling time before relative stability. The theoretical QHARS value near 20.6 MΩ is shown as a red dashed line, and the blue dashed line is the average of a set of DSB measurements. The blue shaded area indicates the standard deviation of the mean of those measurements. Error bars represent the combined standard uncertainty ($k = 1$).

time-dependent measurement validates the stability of this technique for these high resistances, after some time for settling, with some deviations only being off by a few parts in $10^7$. The final test is to prove the concept that this 1.01-MΩ device, while in the Y-network configuration, can exhibit the mathematically transformed value of resistance.

### *B. Proof of Concept for $Y$–$\Delta$ Transformations*

For the final test of the $Y$–$\Delta$ transformation, the test voltage applied to the array was limited to a maximum of 10 V in order to protect cryostat wiring. Based on the transformation calculation, a value near 20.6 MΩ was predicted to be exhibited by the QHARS device when in a proper configuration. This value prompted the use of a 10-MΩ resistor, meaning an applied voltage ratio of about 2.06:1 could be applied. The time-dependent results of this measurement are shown in Fig. 3 (minus the first two points that fall off-scale but suggest a settling time of about 1.5 h). Since the nominal value for the plots and calculations was defined to be 20.6 MΩ exactly, a correction of 1812.6 $\mu\Omega/\Omega$ should be applied to the vertical axis when calculating an absolute deviation from the quantum mechanical value (i.e., the exact QHARS value near 20.6 MΩ). This exact value is demarcated as a red dashed line, and the blue dashed line is the average DSB result that excludes the initial settling measurement. The blue shaded indicates the standard deviation of the mean of those measurements.

The 5-$\mu\Omega/\Omega$ offset from the theoretical value in the proof of principle experimental results may be attributed to the rudimentary DSB-to-QHARS connections where voltage differences at the connections to the QHARS are critical. Improvement to the bridge ground connection by using tetrahedral junctions and additional shielding would reduce lead resistance, thermals, and voltage drops for the measurement of the $Y$–$\Delta$ transformed QHARS. The current to $R_0$ flows mostly in one lead from the QHARS device (specific to the magnetic field orientation) and should be connected as close to the Lo terminal of $V_2$ as possible. A new ground junction box has been designed to improve the DSB-to-QHARS connection at the Gnd terminal using several tetrahedral junctions, which have been used in resistance standards to reduce cross-junction resistance to $2 \times 10^{-7}$ Ω or less [32]. In addition, the 1-MΩ/100-kΩ and the 10-MΩ/1-MΩ ratios were measured for the standard resistors (calibrated with CCC) on the DSB to investigate the 5-$\mu\Omega/\Omega$ offset. Since this test did not reproduce the offset, one cannot correlate it to the worst-case (maximum) 0.1-$\mu\Omega/\Omega$ internal resistance of $V_2$.

One major source of uncertainty at 20.6 MΩ is the instability of the resistance ratio over long times. It is difficult to clearly assign this instability, despite its linearity, to the bridge connections and grounding circuit, but it is at least suggestive given the similar drift that occurs slowly (that is, over the course of hours). It is possible that thermal voltages fluctuate with similar time scales. In the event that one can optimistically treat this linearity as a systematic and predictable error, despite not knowing its origin with full certainty, it may be possible to mitigate or, in the less optimal case, use it to correct measured data.

For now, the best case of calculating any deviation from the nominal value will inherently be dependent on the time of the measurement. The results in Fig. 3 were used to calculate the standard deviation of the mean, which itself has the future potential to be reduced to uncertainties of about 1 $\mu\Omega/\Omega$ (or better should the drift issue be fully understood). Note that the difference in the two measurement types was measured to be approximately 0.23 $\mu\Omega/\Omega$. Considering that typical 10- and 100-MΩ calibration measurements yield standard uncertainties of 1.3 and 1.6 $\mu\Omega/\Omega$, these results highlight the proof of concept that the $Y$–$\Delta$ transformation may be used to drastically reduce the calibration chain as well as provide a means to generate new quantum standards with many accessible high resistances depending on the measurement configuration.

One point of improvement for future devices and metrological studies would be to focus on maintaining the highest material quality for the relatively smaller arm (Gnd). Furthermore, the use of a connector like those used in Hamon networks is critical to reduce errors for the $R_0$ resistor, which is more comparable to the resistance of the leads and connections than the other two arms. The use of the equalizing (four-way) connector would provide a better grounding, as defined by that of the bridge. In this case, any error stemming from the single quantum Hall element would have more drastic error ramifications due to the resistance's placement in the denominator of the $Y$–$\Delta$ transformation.

### *C. Star–Mesh Transformations for Future Quantum Standards*

When inspecting two resistance networks containing $n$ terminals, like the one shown in Figs. 1(a) and 4, one can derive a mathematical relationship between a star network [that is, all arms meeting at a central node like the left side of Figs. 1(a) and 4] and its equivalent mesh network

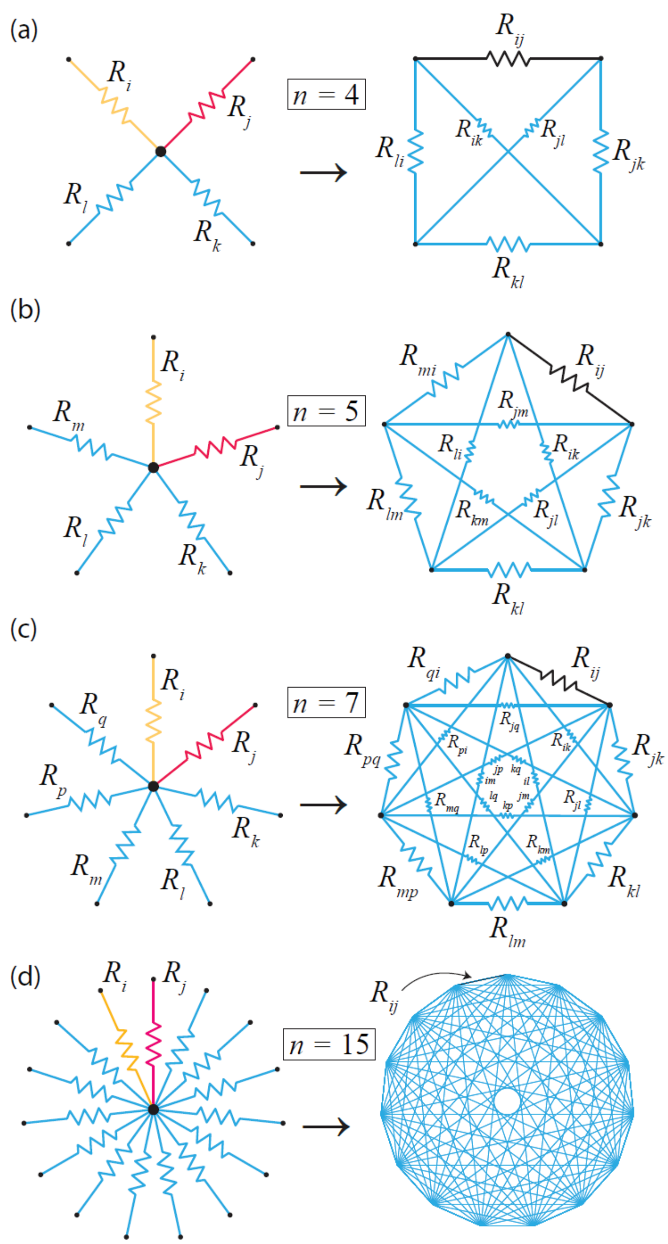


Fig. 4. (a) Four terminal star being transformed to a square mesh with four nodes. (b) Five-terminal star transformed into a pentagonal mesh. (c) Seven-terminal star transformed into a heptagonal mesh. (d) Star–mesh transformation for a 10-GΩ quantum electrical standard is illustrated, representing a possible configuration that is within fabrication capacities, as shown in other works. The exact details of the configuration are provided in Table II. Two of the 15 resistors in the star network are series arrays of several hundred resistors, and the other 13 resistors are single Hall bar elements in parallel. For all subfigures, the uniform cyan color indicates the same potential, like ground as in this study, and applies to all mesh resistors except the high quantized resistance of interest.

[where $n$ is the same, but there exists one fewer node like the right side of Figs. 1(a) and 4] [26], [34], [35]

$$R_{ik} = R_i R_k \sum_{\alpha=1}^{n} \frac{1}{R_\alpha}. \tag{2}$$

In (2), the indices go as high as $n$ and $i \neq k$. To double-check the validity of this generalization, one can derive (1) in a straightforward manner (using $i$, $j$, and $k$ as the indices).

TABLE II

APPLICABLE STAR–MESH TRANSFORMATIONS FOR FUTURE QHARS DEVICES

| $R_i$ (elements) | $R_j$ (elements) | $R_k - R_n$ (single-elements in parallel) | Total (elements) | R (MΩ) |
|---|---|---|---|---|
| 44 | 43 | 2 | 89 | 49.9607 |
| 50 | 50 | 3 | 103 | 98.0887 |
| 44 | 44 | 4 | 92 | 101.083 |
| 49 | 47 | 5 | 101 | 149.856 |
| 44 | 43 | 6 | 93 | 99.9407 |
| 139 | 139 | 4 | 282 | 1 001.05 |
| 188 | 187 | 11 | 386 | 4 995.95 |
| 244 | 244 | 13 | 501 | 9 995.44 |
| 245 | 244 | 13 | 502 | 10 036.4 |

When a star has more than three terminals, it may also follow, for all indices, that

$$\frac{R_{jk}}{R_{ik}} = \frac{R_{jl}}{R_{il}}. \tag{3}$$

This condition must only be met in the event one wishes to transform a mesh to an equivalent star, and such a transformation is not always guaranteed. If one applies (2) to Fig. 4(a) ($n = 4$), then

$$R_{ij} = R_i + R_j + \frac{R_i R_j}{R_k} + \frac{R_i R_j}{R_l}. \tag{4}$$

Just as in this main experimental work, by adding a similarly small resistor in parallel for two of the star arms, the equivalent resistance from the $Y$–$\Delta$ configuration nearly doubles. This favorable multiplicative attribute enables one to build quantum electrical standards with resistances as high as 10 GΩ, as shown in Table II, especially since 13 parallel Hall bar elements have been demonstrated before [7], as have QHARS devices with 236 elements [14].

A star–mesh transformation for a 10-GΩ quantum standard is illustrated in Fig. 4(d). Additional illustrations of potential circuit diagrams using a different star type are provided in the Appendix. Finally, potential configurations are provided in Table II to show how adaptable this method is for high-resistance traceability. One example of the potential of element reduction comes from the 10-GΩ case, where $7.75 \times 10^5$ elements in series are reduced, by means of the star–mesh transformation, to merely 502 elements.

## V. CONCLUSION

A 1.01-MΩ graphene-based QHARS device has been fabricated and shown to operate as an equivalent quantized resistor valued at about 20.6 MΩ by means of using a $Y$–$\Delta$ transformation and corresponding measurement configuration. This potent combination of using graphene-based technology with a mathematical transformation provides a way to extend QHR standards three decades beyond the 1-MΩ range. Additional values that may be attainable reach as high as 10 GΩ, rendering the $Y$–$\Delta$ transformation an incredibly efficient tool for reducing the required number of quantum Hall elements in

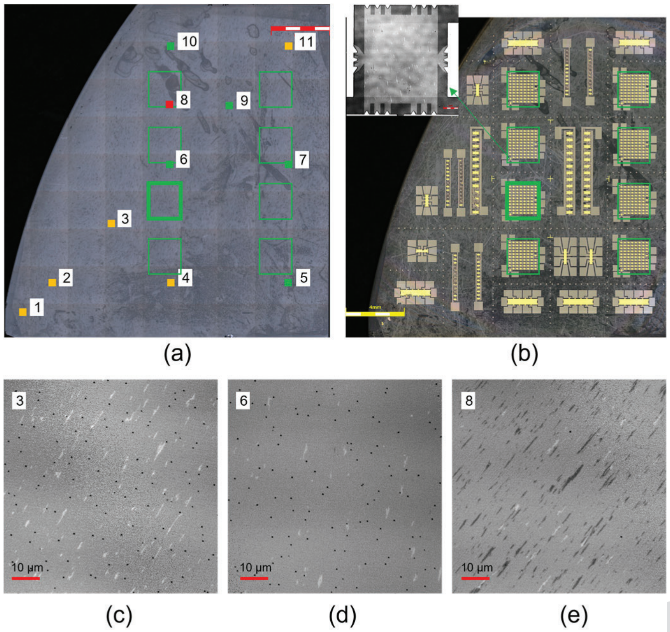


Fig. 5. (a) Optical image is shown of the full-SiC chip with EG before fabrication. The red scale bar at the top right corner represents 4 mm. (b) Same region is shown in postfabrication. The yellow scale bar at the left bottom corner represents 4 mm. (c) Confocal images are shown for: site 3 (orange spot) showing full-monolayer EG coverage with some multilayers. (d) Site 6 (green square) showing minimal multilayer graphene. (e) Site 8 (red spot) showing incomplete monolayer EG with some existing buffer layer.

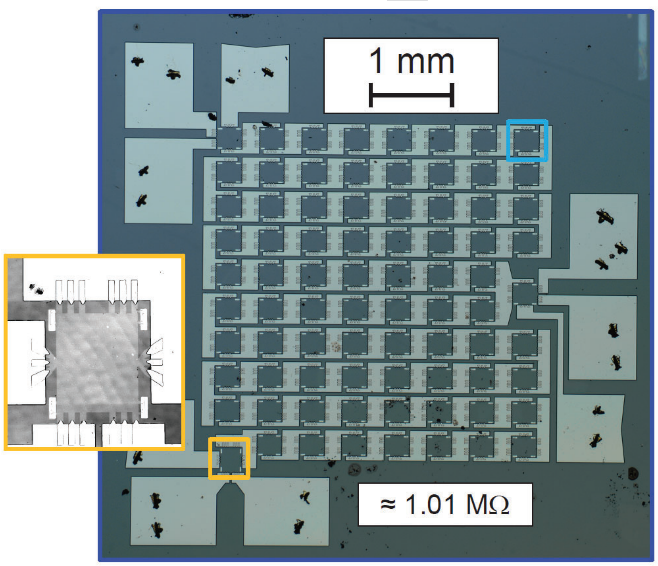


Fig. 6. Optical image of an example device. The inset for the orange region is also provided to demonstrate both the multiseries connections and the clarity with which CLSM successfully identifies EG monolayers.

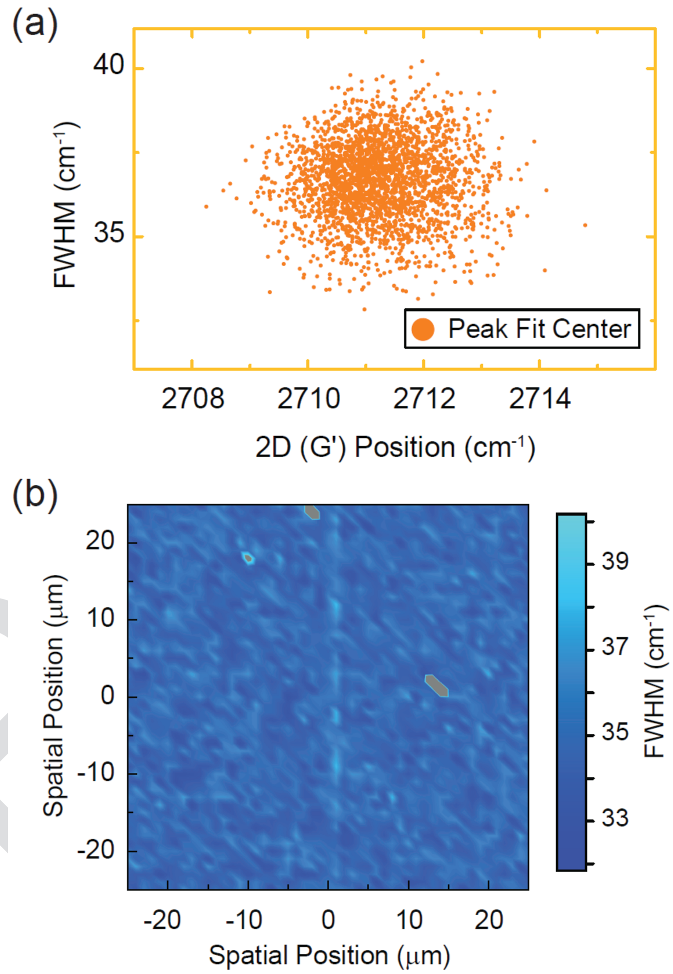


Fig. 7. (a) Scatterplot of the 2-D ($G'$ ) Raman mode of graphene places peak position ($k$-space) against FWHM, helping to verify homogeneity. Each measured peak was fit with a Lorentzian profile. (b) Spatial map of the FWHM for the light blue box in Fig. 6 demonstrates the uniformity of the EG film. Three gray spots indicate minor bilayer growths that generally do not affect the quality of electrical measurements.

series, at least, for resistances higher than 1 MΩ. The results presented herein are a proof of the concept that this type of circuit is beneficial to future resistance metrology applications.

## Appendix

### A. Optical Characterization

Various optical images of example devices are shown in Figs. 5 and 6, with a light blue and orange regions in the latter indicating the two example Hall elements whose Raman map results are shown in Fig. 7(a) and (b), respectively.

For robust statistics on the quality of the EG films, rectangular Raman maps were collected with step sizes of 1 $\mu$m in a 25 $\times$ 25 raster-style grid and repeated on the two outermost corner elements of an example array device. Each spectrum exhibited a clear 2-D ($G'$) peak, which was subsequently fit with a Lorentzian profile to extract a peak position and full-width at half-maximum (FWHM). These quantities were used as the primary metric for comparing EG quality across the devices. It should be noted that the $D$ and $G$ peaks were not selected for determining homogeneity because their spectral neighborhood is strongly dominated by optical responses from the SiC substrate [24]. The resulting scatterplot for one of the elements is shown in Fig. 7(a). For the other elements [Fig. 7(b)], a spatial map is presented with values of the FWHM to give a better visualization of the variation in optical response within that region. Three gray spots on this map represent minor bilayer growths that generally do not affect the quality of electrical measurements. Overall, these data confirm the length scales on which EG can be grown with excellent quality.

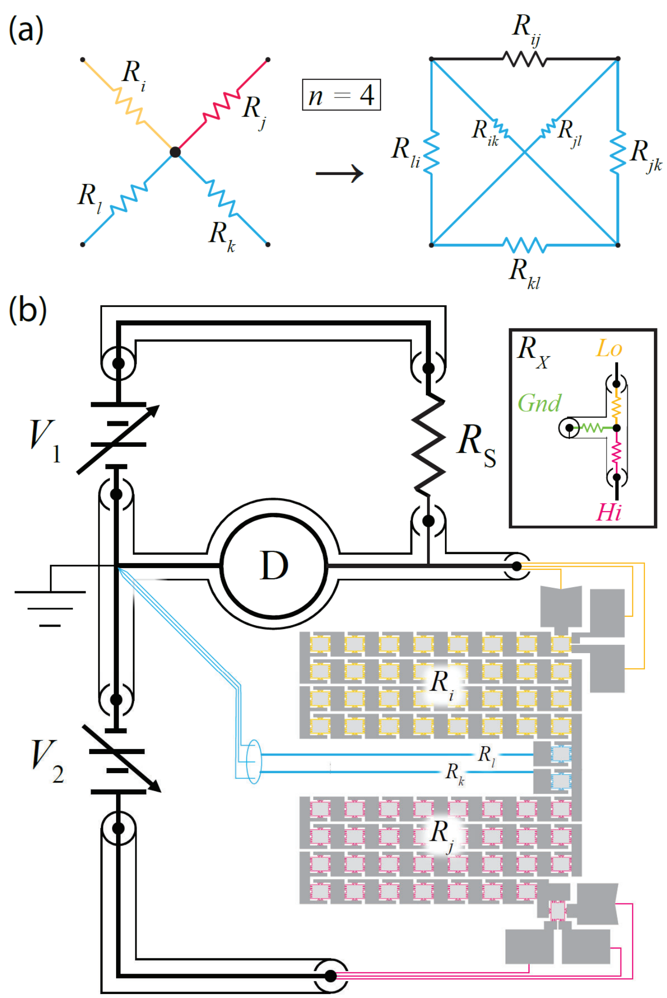


Fig. 8. (a) Four-terminal star being transformed into a square mesh with four nodes. (b) Simplified DSB diagram for a different QHARS. The device, calculated to provide a transformed value of 27.3 MΩ (and presumed to measure 0.826 MΩ across the sum of $R_i$ and $R_j$) and drawn for sake of example, is intended to substitute $R_X$ (see upper inset), with each of its two arrays, composed of 32 elements each and connected in series, meeting at a common node with two distinct and additional branches, each containing a single element. The single element represents the Gnd (or $R_0$, color-coded cyan), whereas the two larger arms make up the Lo and Hi ($R_1$ and $R_2$, respectively) terminal connections.

### *B. Future Circuit Example*

Other circuit designs could implement additional parallel branches with contact pads that are bonded together during fabrication. One such example is shown in Fig. 8. In this case, the device is presumed to measure 0.826 MΩ across the sum of $R_i$ and $R_j$, but after performing a star–mesh transformation, is calculated to provide a value of about 27.3 MΩ. This example device is composed of 32 elements for each of two larger branches and connects in series with a common node that also meets with two distinct and additional branches, each containing a single element. The single element represents the Gnd (or $R_0$, color-coded cyan), whereas the two larger arms make up the Lo and Hi ($R_1$ and $R_2$, respectively) terminal connections. Though these values were arbitrarily chosen, the exemplify a benefit in using additional grounded branches as a means to reduce the number of required devices to achieve large transformed quantized resistances.

## ACKNOWLEDGMENT

The authors would like to thank L. Chao, F. Fei, and E. C. Benck for their assistance during the internal review process at NIST. The work of S. Mhatre and C.-C. Yeh at the National Institute of Standards and Technology (NIST), Gaithersburg, MD, USA, was made possible by arrangement with Prof. C.-T. Liang of National Taiwan University, Taipei City, Taiwan. Certain commercial equipment, instruments, or materials are identified in this article to foster understanding. Such identification neither imply recommendation or endorsement by the National Institute of Standards and Technology or the U.S. Government nor does it imply that the materials or equipment identified are necessarily the best available for the purpose.

## REFERENCES

[1] T. J. B. M. Janssen et al., "Precision comparison of the quantum Hall effect in graphene and gallium arsenide," *Metrologia*, vol. 49, no. 3, pp. 294–306, Jun. 2012.

[2] J. Kucera, P. Svoboda, and K. Pierz, "AC and DC quantum Hall measurements in GaAs-based devices at temperatures up to 4.2 K," *IEEE Trans. Instrum. Meas.*, vol. 68, no. 6, pp. 2106–2112, Jun. 2019.

[3] A. F. Rigosi and R. E. Elmquist, "The quantum Hall effect in the era of the new Si," *Semicond. Sci. Technol.*, vol. 34, no. 9, Sep. 2019, Art. no. 093004.

[4] A. Tzalenchuk et al., "Towards a quantum resistance standard based on epitaxial graphene," *Nature Nanotechnol.*, vol. 5, no. 3, pp. 186–189, Mar. 2010.

[5] M. Woszczyna et al., "Precision quantization of Hall resistance in transferred graphene," *Appl. Phys. Lett.*, vol. 100, no. 16, Apr. 2012, Art. no. 164106.

[6] T. Oe et al., "Comparison between NIST graphene and AIST GaAs quantized Hall devices," *IEEE Trans. Instrum. Meas.*, vol. 69, no. 6, pp. 3103–3108, Jun. 2020.

[7] A. R. Panna et al., "Graphene quantum Hall effect parallel resistance arrays," *Phys. Rev. B, Condens. Matter*, vol. 103, no. 7, Feb. 2021, Art. no. 075408.

[8] T. Oe, S. Gorwadkar, T. Itatani, and N. Kaneko, "Development of 1 MΩ quantum Hall array resistance standards," *IEEE Trans. Instrum. Meas.*, vol. 66, no. 6, pp. 1475–1481, Jun. 2017.

[9] M. Kruskopf et al., "Next-generation crossover-free quantum Hall arrays with superconducting interconnections," *Metrologia*, vol. 56, no. 6, Dec. 2019, Art. no. 065002.

[10] M. Kruskopf et al., "Two-terminal and multi-terminal designs for next-generation quantized Hall resistance standards: Contact material and geometry," *IEEE Trans. Electron Devices*, vol. 66, no. 9, pp. 3973–3977, Sep. 2019.

[11] A. Lartsev, S. Lara-Avila, A. Danilov, S. Kubatkin, A. Tzalenchuk, and R. Yakimova, "A prototype of RK/200 quantum Hall array resistance standard on epitaxial graphene," *J. Appl. Phys.*, vol. 118, no. 4, Jul. 2015, Art. no. 044506.

[12] S. Novikov et al., "Mini array of quantum Hall devices based on epitaxial graphene," *J. Appl. Phys.*, vol. 119, no. 17, May 2016, Art. no. 174504.

[13] J. Park, W.-S. Kim, and D.-H. Chae, "Realization of $5\frac{h}{e^2}$ with graphene quantum Hall resistance array," *Appl. Phys. Lett.*, vol. 116, no. 9, Mar. 2020, Art. no. 093102.

[14] H. He et al., "Accurate graphene quantum Hall arrays for the new international system of units," *Nature Commun.*, vol. 13, no. 1, p. 6933, Nov. 2022.

[15] K. M. Yu, D. G. Jarrett, A. F. Rigosi, S. U. Payagala, and M. E. Kraft, "Comparison of multiple methods for obtaining PΩ resistances with low uncertainties," *IEEE Trans. Instrum. Meas.*, vol. 69, no. 6, pp. 3729–3738, Jun. 2020.

[16] H. A. Sauer, "Wye-delta transfer standards for calibration of wide range DC resistance and DC conductance bridges," *IEEE Trans. Instrum. Meas.*, vol. IM-17, no. 2, pp. 151–155, 1968.

[17] F. L. Hernandez-Marquez, M. E. Bierzychudek, G. R. Jones, and R. E. Elmquist, "Precision high-value resistance scaling with a two-terminal cryogenic current comparator," *Rev. Sci. Instrum.*, vol. 85, no. 4, Apr. 2014, Art. no. 044701.

[18] M. Kruskopf et al., "Graphene quantum Hall effect devices for AC and DC electrical metrology," *IEEE Trans. Electron Devices*, vol. 68, no. 7, pp. 3672–3677, Jul. 2021.

[19] V. Panchal et al., "Confocal laser scanning microscopy for rapid optical characterization of graphene," *Commun. Phys.*, vol. 1, no. 1, p. 83, Nov. 2018.

[20] M. A. Real et al., "Graphene epitaxial growth on SiC(0001) for resistance standards," *IEEE Trans. Instrum. Meas.*, vol. 62, no. 6, pp. 1454–1460, Jun. 2013.

[21] A. F. Rigosi et al., "Analytical determination of atypical quantized resistances in graphene p-n junctions," *Phys. B, Condens. Matter*, vol. 582, Apr. 2020, Art. no. 411971.

[22] S. M. Mhatre et al., "Dynamics of transient hole doping in epitaxial graphene," *Phys. Rev. B, Condens. Matter*, vol. 105, no. 20, May 2022, Art. no. 205423.

[23] T. J. B. M. Janssen et al., "Anomalously strong pinning of the filling factor $v = 2$ in epitaxial graphene," *Phys. Rev. B, Condens. Matter*, vol. 83, no. 23, Jun. 2011, Art. no. 233402.

[24] H. M. Hill et al., "Probing the dielectric response of the interfacial buffer layer in epitaxial graphene via optical spectroscopy," *Phys. Rev. B, Condens. Matter*, vol. 96, no. 19, Nov. 2017, Art. no. 195437.

AQ:7 [25] A. E. Kennelly, "Equivalence of triangles and stars in conducting networks," in *The Electrical World and Engineer*, vol. 34. 1899, pp. 413–414.

[26] L. Versfeld, "Remarks on star-mesh transformation of electrical networks," *Electron. Lett.*, vol. 19, no. 6, pp. 597–599, 1970.

[27] V. V. B. Rao and V. K. Aatre, "Mesh-star transformation," *Electron. Lett.*, vol. 6, no. 10, pp. 73–74, 1974.

[28] D. G. Jarrett, "Automated guarded bridge for calibration of multimegohm standard resistors from 10 MΩ to 1 TΩ," *IEEE Trans. Instrum. Meas.*, vol. 46, no. 2, pp. 325–328, Apr. 1997.

AQ:8 [29] D. G. Jarrett et al., "Graphene quantized Hall arrays as wye-delta transfer standards," in *Proc. Conf. Precis. Electromagn. Meas. (CPEM)*, 2023.

[30] L. C. A. Henderson, "A new technique for the automatic measurement of high value resistors," *J. Phys. E, Sci. Instrum.*, vol. 20, no. 5, pp. 492–495, May 1987.

[31] G. Rietveld, D. Jarrett, and B. Jeckelmann, "Accurate high-ohmic resistance measurement techniques up to 1 PΩ," in *Proc. 29th Conf. Precis. Electromagn. Meas. (CPEM)*, Aug. 2014, pp. 290–291.

[32] C. H. Page, "Tetrahedral junction error contribution to a series-parallel four-terminal resistor," *IEEE Trans. Instrum. Meas.*, vol. IM-23, no. 1, pp. 5–8, Mar. 1974.

[33] J. Konemann, F. Ahlers, E. Pesel, K. Pierz, and H. W. Schumacher, "Magnetic field reversible serial quantum Hall arrays," *IEEE Trans. Instrum. Meas.*, vol. 60, no. 7, pp. 2512–2516, Jul. 2011.

[34] K. Kupfmuller, *Einführung in Die Theoretische Elektrotechnik*. Berlin, Germany: Springer, 1968.

[35] R. E. Scott, *Linear Circuits*. Reading, MA, USA: Addison-Wesley, 1960.


**Dean G. Jarrett** (Senior Member, IEEE) was born in Baltimore, MD, USA, in 1967. He received the B.S. degree in electrical engineering from the University of Maryland, College Park, MD, USA, in 1990, and the M.S. degrees in electrical engineering and applied biomedical engineering from Johns Hopkins University, Baltimore, in 1995 and 2008, respectively.

Since 1986, he has been with the National Institute of Standards and Technology (NIST), Gaithersburg, MD, USA, where he was a Cooperative Education Student with the University of Maryland. During this time, he worked in the dc resistance area on the automation of resistance calibration systems. In 1991, he joined NIST, as a full-time Electrical Engineer working on the development of an automated ac resistance calibration system and the development of new resistance standards. Since 1994, he has been working in the high-resistance laboratory developing automated measurement systems and improving standard resistors to support high-resistance calibration services and key comparisons. In recent years, he has worked on sensor technologies for the detection of biological molecules and low-current source and measure techniques. Since 2014, he has been leading the Metrology of the Ohm Project at NIST.

**Ching-Chen Yeh** received the B.S. degree in physics from Chung Yuan Christian University, Taoyuan City, Taiwan, in 2017, and the M.S. degree in physics from National Taiwan University, Taipei City, Taiwan, in 2019, where he is currently pursuing the Ph.D. degree.

He is currently a Guest Researcher with the National Institute of Standards and Technology (NIST), Gaithersburg, MD, USA.

**Shamith U. Payagala** received the B.S. degree in electrical engineering from the University of Maryland, College Park, MD, USA, in 2015, and the M.S. degree in electrical engineering from Johns Hopkins University, Baltimore, MD, USA, in 2019.

In 2014, he joined the National Institute of Standards and Technology (NIST), Gaithersburg, MD, USA, as an Electrical Engineer for the Metrology of the Ohm Project. His research interests include direct current comparator bridges, improving the repeatability of ultrahigh resistance measurements using dual-source bridges (DSBs), ultralow current amplifier systems for low-current generation and measurements, advancing capabilities of temperature-controlled chambers, and graphene-based quantized Hall resistance (QHR) standards using cryogen-free cryocoolers.

**Alireza R. Panna** was born in Mumbai, India. He received the B.S. degree in electrical engineering from the University of Maryland, College Park, MD, USA, in 2013.

From 2012 to 2013, he was a Guest Researcher with the National Institute of Standards and Technology (NIST), Gaithersburg, MD, where he was involved in magnet characterization for the NIST-4 watt balance. From 2013 to 2017, he was with the National Institutes of Health, Bethesda, MD, USA, where he worked on controls and characterization of various X-ray imaging modalities. He is currently with the NIST, where he is involved in the Metrology of the Ohm and the Quantum Conductance Projects.

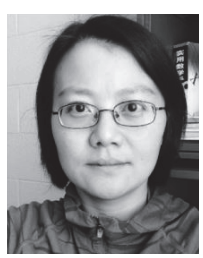

**Yanfei Yang** (Member, IEEE) received the B.S. degree in applied optics from Sichuan University, Chengdu, China, in 1999, and the Ph.D. degree in physics from Georgetown University, Washington, DC, USA, in 2010. Her Ph.D. thesis focused on quantum transport in carbon nanotubes and the investigation of possible intrinsic superconductivity in isolated carbon nanotubes.

She was an Associate Researcher with the National Institute of Standards and Technology (NIST), Gaithersburg, MD, USA, from 2012 to 2017, where she had been involved in the development of new resistance standards based on quantum Hall devices made of epitaxial graphene.

Dr. Yang was awarded the Physical Measurement Laboratory's (NIST) Distinguished Associated Award for advancing quantum metrology through the development of graphene quantum Hall resistance standards that offer robust, accurate, and cost-effective dissemination of the ohm.

**Linli Meng** received the B.S. and M.S. degrees in material physics from Sichuan University, Chengdu, China, and the Ph.D. degree in materials science from the University of Minnesota, Twin Cities, MN, USA, in 2008.

After graduation, she joined the OFS Laboratories, Somerset, NJ, USA, and was involved in photonic bandgap optical fibers research and development. In 2017, she co-founded Graphene Waves, LLC, Gaithersburg, MD, USA, with Yanfei Yang. She is currently the Chief Technology Officer of Graphene Waves, LLC. Her research interests include epitaxial graphene and quantum devices based on epitaxial graphene.

**Swapnil M. Mhatre** received the B.E. degree in electronics and instrumentation engineering and the M.S. degree in physics from the Birla Institute of Technology and Science, Pilani, India, in 2017, and the Ph.D. degree in applied physics from National Taiwan University, Taipei City, Taiwan, in 2022. His Ph.D. thesis focused on quantum transport in the quantum Hall regime for epitaxial graphene and its applications to metrology and discussed the doping mechanism of epitaxial graphene using nitric acid.

He was a Guest Researcher with the National Institute of Standards and Technology (NIST), Gaithersburg, MD, USA, working on quantum Hall resistance standards based on epitaxial graphene, from 2021 to 2022. He is currently a Post-Doctoral Associate with the University of Colorado, Boulder, CO, USA, where he is exploring the effect of cavities on ultra-thin oxide MIM junction devices.

**Ngoc Thanh Mai Tran** was born in Ho Chi Minh City, Vietnam, in 1992. She received the B.Sc. and M.Sc. degrees in electronic engineering from the Politecnico di Torino, Turin, Italy, in 2014 and 2017, respectively, and the Ph.D. degree in metrology from the Politecnico di Torino and the Istituto Nazionale di Ricerca Metrologica, Turin. She did her master's thesis at the National Metrology Institute of Japan (NMIJ), Tsukuba, Japan.

She was a Guest Researcher with the Korea Research Institute of Standards and Science (KRISS), Daejeon, South Korea. She is currently a Post-Doctoral Research Associate with the National Institute of Standards and Technology, Gaithersburg, MD, USA, and is involved in several projects related to the metrology of electrical resistance and impedance.

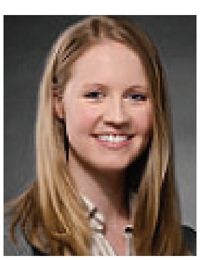

**Heather M. Hill** received the B.S. degree in physics from Duke University, Durham, NC, USA, in 2011, and the M.A., M.Phil., and Ph.D. degrees in physics from Columbia University, New York, NY, USA, in 2013, 2014, and 2016, respectively.

From 2016 to 2018, she was a Physicist with the National Institute of Standards and Technology (NIST), Gaithersburg, MD, USA, and a fellow of the National Research Council Research Associateship Program studying 2-D materials and their optical properties. She is currently a Guest Researcher with NIST and affiliated with the American Institute of Physics.

Dr. Hill is a member of the American Physical Society. She was previously awarded a National Science Foundation IGERT Grant.

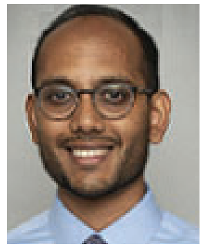

**Dipanjan Saha** received the B.S. degree in mechanical engineering and biomedical engineering from the University of Connecticut, Mansfield, CT, USA, and the Ph.D. degree in mechanical engineering from Carnegie Mellon University, Pittsburgh, PA, USA.

From 2020 to 2022, he was a Post-Doctoral Researcher with the National Institute of Standards and Technology (NIST), Gaithersburg, MD, USA, conducting research on various graphene technologies in the application spaces of metrology and optoelectronics. He is currently a Senior Principal Physicist with Northrop Grumman Corporation, Linthicum, MD, USA, researching superconducting electronics for advanced computing applications.

**Randolph E. Elmquist** (Senior Member, IEEE) received the Ph.D. degree in physics from the University of Virginia, Charlottesville, VA, USA, in 1986.

He leads the Quantum Conductance Project at the National Institute of Standards and Technology (NIST), Gaithersburg, MD, USA. Working for the past 32 years in the field of electrical and quantum metrology, he has contributed to the experimental design and measurement of the electronic kilogram and calculable impedance standards for the determination of the von Klitzing constant and alpha, the unitless fine structure constant. He leads the development of cryogenic current comparator (CCC) systems, the quantum Hall effect, and graphene electronic devices for metrology.

Dr. Elmquist is a member of the American Physical Society.

**David B. Newell** received the B.S. degree in physics and the B.A. degree in mathematics from the University of Washington, Seattle, WA, USA, and the Ph.D. degree in physics from the University of Colorado, Boulder, CO, USA.

He became a full-time Staff Member with the National Institute of Standards and Technology (NIST), Gaithersburg, MD, USA, in 1996. He has worked on measurements for realizing micro- and nanoscale forces traceable to the SI, was the Leader of the Fundamental Electrical Measurements (FEM) Group, from 2004 to 2010, helped establish the use of graphene in quantum electrical standards, worked with a NIST Team to construct a new watt balance to realize the kilogram from a fixed value of the Planck constant, and, as the Chair of the CODATA Task Group on Fundamental Constants, provided the exact values of the fundamental constants to be used in the new SI. He has presently again accepted responsibility as the Leader of the FEM Group.

Dr. Newell is a member of the Philosophical Society of Washington, the Chair of the CODATA Task Group on Fundamental constants, and a fellow of the American Physical Society. He was awarded the NRC Post-Doctoral Fellowship to work on the Watt Balance Project at NIST.

**Albert F. Rigosi** (Member, IEEE) was born in New York, NY, USA. He received the B.A., M.A., M.Phil., and Ph.D. degrees in physics from Columbia University, New York, in 2011, 2013, 2014, and 2016, respectively.

From 2008 to 2015, he was a Research Assistant with the Columbia Nano Initiative, New York. From 2015 to 2016, he was a Joint Visiting Research Scholar with the Department of Applied Physics, Stanford University, Stanford, CA, USA, and the PULSE Institute of SLAC National Accelerator Laboratory, Menlo Park, CA, USA. Since 2016, he has been a Physicist with the National Institute of Standards and Technology, Gaithersburg, MD, USA. His research interests include 2-D electron systems and applications of those systems' behaviors for electrical metrology.

Dr. Rigosi is a member of the American Physical Society and the Mellon-Mays Initiative of The Andrew W. Mellon Foundation. He was awarded the associateships and fellowships from the National Research Council (USA), the Optical Society of America, the Ford Foundation, and the National Science Foundation (Graduate Research Fellowship Program).